SEMARAK ILMU PUBLISHING

Journal of Advanced Research in Fluid Mechanics and Thermal Sciences

Journal homepage:
https://semarakilmu.com.my/journals/index.php/fluid_mechanics_thermal_sciences/index
ISSN: 2289-7879

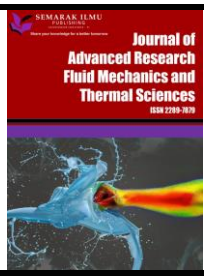

Effect of Indoor Condition with Cross Ventilation on Deposition of Airborne Droplets Emitted from Human Cough

Stanferd Jenta Sanada[1], Mohamad Nur Hidayat Mat[1,*]

[1] School of Mechanical Engineering, Faculty of Engineering, Universiti Teknologi Malaysia, 81310 UTM Johor Bahru, Malaysia

ARTICLE INFO

Article history:
Received 8 August 2022
Received in revised form 13 December 2022
Accepted 22 December 2022
Available online 9 January 2023

Keywords:
Airborne transmission; cross ventilation; discrete phase model; droplet deposition; Euler-Lagrange

ABSTRACT

Prediction of airborne transmission in different environmental condition remains as the research challenge in the field. This has motivated the present study to obtain the direct impact of flow field to the physical nature of transmission. ANSYS Fluent 2022 R1 software is utilised in this research to numerically investigate and visualize flow pattern in a closed environment with cross ventilation and its effect to the emitted droplets deposition. The effect of different indoor parameters towards airborne transmission are investigated, which include wind velocity, air relative humidity (RH), and exposure time after emission. Simulation result revealed increasing wind velocity according to Beaufort wind scale of 1.0 to 3.9 m/s, increases transmission rate due to enhanced convection effect. Surrounding air with higher RH leads to a larger mean diameter of particles due to hygroscopic growth effect, while evaporation effect dominates in lower air RH, leading to particle shrinkage. In a light wind breeze, droplet mass of 5.15 mg deposited on receiver body within 0.5 s of transmission when RH is 40%, while only 3.29 mg droplets reached receiver in RH of 99.5%. Droplet particles settle on the floor within 1.50 s revealed 0.66 mg deposited mass in higher RH, while 0.26 mg of droplets deposited in lower RH. Deposition at transmitter body is possible due to recirculation effect of incoming wind generated between transmitter and receiver, leading to 3.7 times higher deposited mass in lower RH as compared to in higher RH. This research highlights application of Euler-Lagrange model to represent the trajectory of cough droplets influenced by indoor condition with horizontal wind, in the effort to strengthen safety and health judgement in the event of a pandemic.

1. Introduction

Airborne pathogen can be dispersed through the surrounding medium of air due to its micron level size. Human respiratory mechanism including coughing and sneezing generates airborne particles which can be classified into two groups. Bigger sized droplets in the range of 5 to 10 µm are considered as respiratory droplets, while those smaller than 5 µm is classified as aerosols [1]. Larger droplets have shorter travel distance and fall to the ground faster, compared to aerosols that can cover a larger distance while being airborne. When smaller droplets evaporate, the virus is left

* *Corresponding author.*
E-mail address: mn.hidayat@utm.my

https://doi.org/10.37934/arfmts.102.1.184202

airborne to the environment. Viruses including COVID-19 from an infected person can be potentially transmitted through physical contact or from contamination of clothing, utensils, and surfaces [2]. In the context of human-to-human transmission, COVID-19 virus can potentially be transmitted from a distance of less than a meter [3]. A thorough knowledge of pathogen transmission behaviour towards the environmental condition remains a challenge in containing the spread of viral disease.

Numerous research effort in the field of airborne transmission is observed since the declaration of COVID-19 as pandemic by WHO. Recent research mostly focusing on the spread of respiratory particles on its infection risk and the mitigation strategies. In contrast to invasive method through vaccine shots, non-pharmaceutical interventions remain as the critical strategy in flattening epidemic curve [4]. In the context of respiratory-emitted pathogens, mode of transmission including breathing, talking, coughing, and sneezing are some of the transmission modes being widely discussed in the literature. Zhang *et al.,* [5] studied the transmission of respiratory aerosols generated from breathing in a public bus. Air change rate level coupled with the HVAC configuration in the bus able to reduce the contaminant concentration. Xi *et al.,* [6] investigated the transport of airborne aerosols in the human upper airway system from wearing face mask. The study focuses on the inhalation and deposition of the viral contaminants in human respiratory organs. Breathing-induced virus-laden particles transmitted dispersed to the surrounding with the effect of facial mask and air flow from ventilation is experimentally investigated by Shah *et al.,* [7]. Indoor condition with stringent ventilation and hygiene requirement such as those in Class 1 operation room is studied through simulation to capture the behaviour of bioaerosols distribution under the influence of supplied air and room temperature [8]. Most literatures focusing on breathing and talking as the transmission mode, with lower number of researchers working on coughing and sneezing mode as the transmission source. Coughing as the transmission source is considered in the present study to explore the flow pattern and particle transmission pattern.

In the context of sustaining indoor air quality and virus spread control, a closed space often equipped with air distribution system, that functions to supply fresh air into the space and vent out existing airborne contaminants. Existing literature from Wong *et al.,* [9] analysed movement of airborne particulate matter in a hospital operation theater. In the study, the application of ventilation is categorized as downward ventilation, which is commonly the case for operation room. Similarly, Hedworth *et al.,* [10] established mitigation strategies for airborne diseases in orchestra hall equipped with downward ventilation. In downward ventilation, lower temperature air enters from a ceiling diffuser with low speed and exits through the outlet vents at opposite wall placed near the floor. In the case of displacement ventilation, air that is cooler than ambient air is supplied from wall inlet placed near the floor, which then rises upwards facilitated by thermal plume from a heat source in the room and exits through the outlet placed near the ceiling. Ji *et al.,* [11] is one of many researchers studied the influence of surrounding air humidity on the dispersion and evaporation of droplets exhaled through breathing cycle of human. Efficiency of mixing ventilation towards contamination risk of SARS-CoV-2 virus in dental clinic is revealed through computational simulation [12]. Similarly, Mariam *et al.,* [13] investigated respiratory-induced airborne transmission in a closed space with mixing ventilation configuration. In contrast to displacement ventilation, a mixing ventilation works by supplying high speed air from a wall near the ceiling level which then mixes with the indoor air and is then vented out of the room through a wall outlet placed near the floor. Computational fluid dynamic simulation performed by Cheong *et al.,* [14] to assess effectiveness of under-floor ventilation in controlling spread of airborne pathogens in a classroom. Most literatures have studied different ventilation mode, with only few of them studying on the stratum or cross ventilation. Present study used stratum ventilation to represent the horizontal wind direction to

capture the continuous phase interaction with the emitted airborne droplets near the breathing level of the contaminant source.

By understanding the relation between the surrounding flow field and the emitted particles, virus-laden pathogens can be further contained and addressed with multiple strategies on hand. While understanding flow pattern is paramount in this study, next strategy is to better understand the dynamics of indoor environment towards pathogen transmission. This is done to address the current insufficient literature in containing spread of airborne diseases in different indoor condition which includes supplied air velocity, air relative humidity, and human factor such as the inter-personal distance. Hence, this study aims to present the influence of indoor condition with horizontal wind towards the deposition direction of droplets emitted from coughing. This objective is supported with graphical visualization of the flow field of the site with its corresponding quantitative analysis.

2. Methodology

2.1 Computational Domain

The computational fluid dynamics (CFD) approach is initiated by designing the computational domain in which the coughing simulation will take place in. Two mannequin models are placed in the domain to represent the coughing person and infected person. The models are enclosed in a space with dimension of W = 3 m, H = 3 m, L = 6 m [15]. A cross ventilation condition is represented by the velocity inlet behind the coughing person (transmitter) and the pressure outlet behind the infected person (receiver) to capture the interaction of inlet wind with the airborne contaminants, as shown in Figure 1.

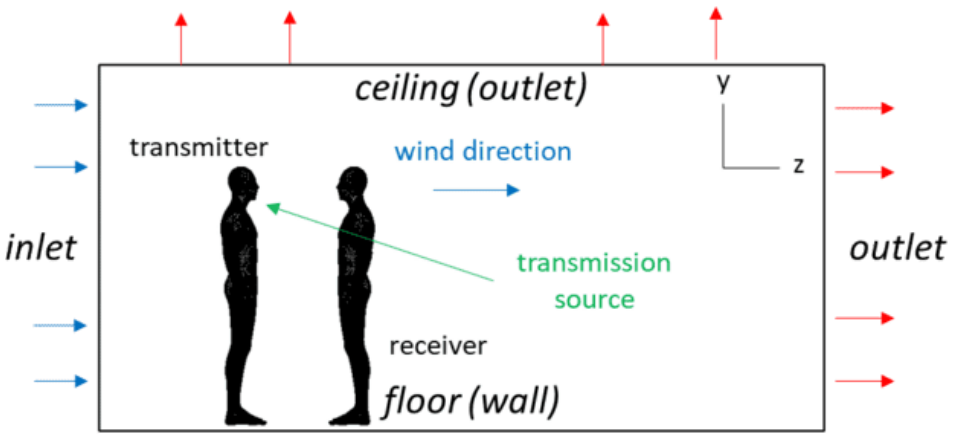

Fig. 1. Transmission source located downstream of inlet wind

Both mannequins are scaled to a height of 1.75 m [16]. A geometrical model is established to represent physical distance of 3 feet (0.91 m), between coughing person (transmitter) and infected person (receiver). The dimension of the computational domain is described in Figure 2.

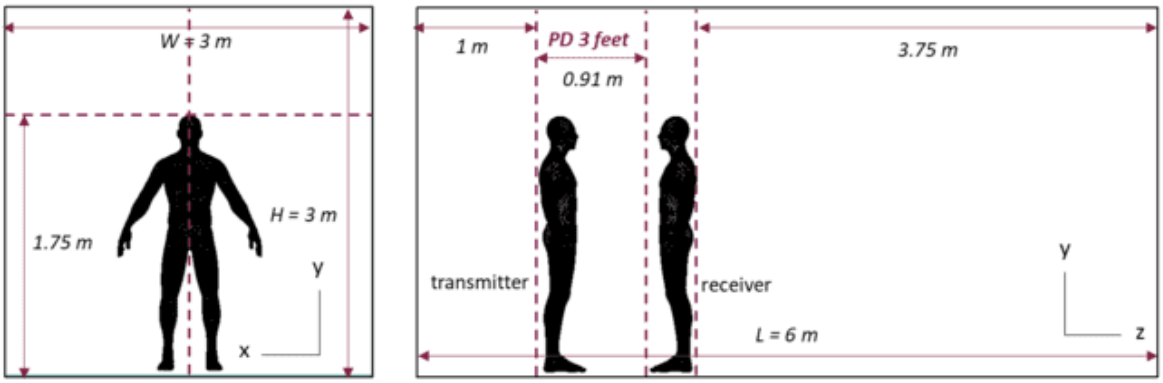

Fig. 2. Computational domain dimension as viewed from xy-plane and yz-plane [17]

Euler-Lagrange multiphase model is adopted in this study to capture transport of particles and its corresponding size change and transmission of infectious droplets [18]. The model is chosen to generate the visualization of air flow and particle transmission in the post-processing phase. Both phases described the continuous phase in Eulerian frame and the discrete phase of the particle in Lagrangian frame [19].

Droplets expelled from coughing is fitted based on Rosin-Rammler particle distribution method. Relationship between Y_d and d is described in Eq. (1), where Y_d is droplet mass fraction with size bigger than particle of diameter d. From the equation, n is the spread parameter and d_n is the mean diameter of droplet, is calculated to generate the corresponding droplet size distribution curve. The effect of droplet sizes on its trajectories is investigated by adopting wide range of cough particles distribution [20]. Two sets of droplet diameter size distribution are used to represent the cough emission droplet size of 1 to 50 µm and 50 to 1000 µm [21].

$$Y_d = e^{-(\frac{d}{d_n})^n} \tag{1}$$

For each of the simulation case, specific parameter is used to represent the air flow distribution and airborne transmission in an enclosed space. Varying indoor parameters include inlet wind velocity, air humidity, and particle exposure time. Discrete phase model (DPM) is adopted in the simulation to capture the dynamics of the emitted particles upon interaction with the air flow. Therefore, the DPM state is defined accordingly at each surface boundary condition for the solver to compute the mass concentration of the deposited droplets. The parameters used in the simulation cases and the boundary condition property is defined in Table 1.

Table 1
Boundary condition setting

Surface	Boundary condition	DPM State	Parameter
Inlet	Velocity inlet	Escape	Wind speed: 1.0, 3.9, 5.5 m/s [22] Air humidity (RH): 40%, 99.5% [20] Air temperature: 27°C [20]
Transmitter's mouth	Velocity inlet	Trap	Transient cough velocity [23] H_2O: 89.6%, NaCl: 10.4% [24]
Walls, ceiling, outlet	Pressure outlet	Escape	0 Pa
Transmitter	Wall	Trap	Heat flux 0 W/m^2
Receiver	Wall	Trap	Heat flux 0 W/m^2
Floor	Wall	Trap	Heat flux 0 W/m^2
Injector tube	Wall	Reflect	Heat flux 0 W/m^2

2.2 Mesh Sensitivity Test

It is important that the accuracy level of geometrical model to be defined before obtaining the final solution. This analysis is done to obtain optimum balance between a fine mesh for highly accurate computation and a data-driven guess on compute time. Each mesh elements are based on sets of governing equations that is solved at the center point of each element. Solution value defined as the axial velocity of the cough jet is referred to value from existing literature. Axial velocity of cough jet calculated at a distance of 14 cm from the injection surface of transmitter's mouth is compared with the reference value of 5.62 m/s [16]. The tendency of numerical result to deviate from actual solution can be eliminated by solving numerical equation at the centroid of each mesh element [25]. In addition, mesh properties including the size and skewness will determine the final result, due to the dependency of its result on the adjacent cells [26]. This test is initiated by performing refinement to the mesh from coarse to medium, and medium to finer meshing. The transmitter and receiver human are modelled as standing mannequin facing each other in an enclosed room. Due to the irregular nature of the mannequin geometry, it is practical to generate an unstructured tetrahedral mesh with respect to the discretization error to fit into the computational domain configuration. Representative cell length, h will then be calculated from the number of elements of each mesh level. For infinitely fine mesh, number of elements, N reaching towards infinite number, while representative cell length, h is approximated to be zero $(h = 0)$. Since the model is three-dimensional, value of h can be calculated from Eq. (2).

Mesh refinement is specified to be at 30% difference between each subsequent meshing refinement [27]. Local mesh refinement for the domain is presented in Figure 3. In the present study, mesh convergence is plotted against the solution value of interest, which is the axial velocity of the cough jet. Each mesh level corresponds to the axial velocity value, which this study used the fine mesh as the final mesh level. Fine mesh corresponds to representative cell length of 10.9 mm, with axial velocity value of 5.46 m/s. The mesh convergence plot is shown in Figure 4.

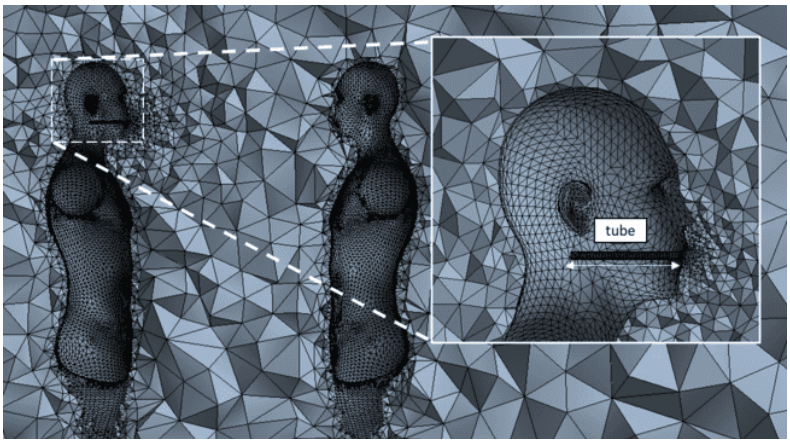

Fig. 3. Mesh refinement at transmitter's mouth tube viewed in y-z plane

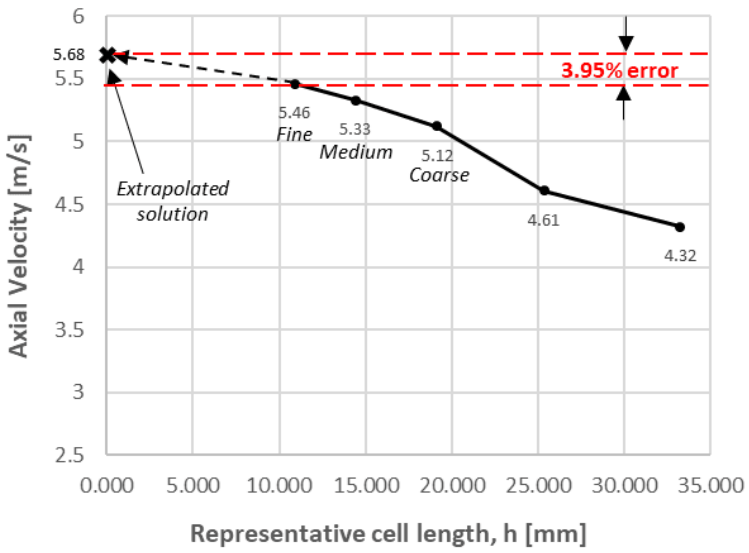

Fig. 4. Mesh convergence plot for axial velocity value

Result from the CFD simulation is expected to have a sufficiently low percentage error when mesh size is infinitely small. In this case, simulation with smallest mesh size is impractical for the present study due to high computing processor requirement. However, a calculation of percentage error is made to evaluate the solution obtained from the present fine mesh, with respect to the extrapolated solution using Richardson extrapolation method. Figure 4 presents the extrapolated relative error between fine mesh solution and extrapolated solution is calculated to be 3.95%, by using Eq. (3), with φ_1 being the extrapolated solution value, and φ_0 is the fine mesh solution value. Hence, h value of 10.9 mm is used, with error below 5%.

$$h = \frac{1}{N}\sum_{Cells} V_p^{\frac{1}{3}} \tag{2}$$

$$e_{21}^{extr} = \left|\frac{\varphi_1 - \varphi_0}{\varphi_0}\right| \tag{3}$$

2.3 Turbulence Model Selection

Fine meshing with corresponding representative cell length, h = 10.9mm is applied through all three computational domain in the CFD simulation. In previous section, a base simulation case adopted the use of k-omega turbulence model for comparison purposes. Other turbulence model including k-epsilon, Spalart-Allmaras, SAS (Scale-Adaptive Simulation), and LES (Large Eddy Simulation) is tested with the fine mesh setting, with axial velocity of cough jet as the solution value of interest. Based on the turbulence model result, the value of axial velocity for k-epsilon model yielded the least amount of error of 1.94%, in relative to the extrapolated solution from Richardson extrapolation method. Hence, the k-epsilon turbulence model with fine mesh setting is used throughout the present study. The solution value of each turbulence model is presented in Table 2.

Table 2
Turbulence model comparison

Model	Axial velocity (m/s)	Extrapolated (m/s)	Error (%)
Spalart-Allmaras	2.90	5.68	48.94
SAS	4.13	5.68	27.29
LES	4.82	5.68	15.14
k-omega	5.46	5.68	3.87
k-epsilon	5.57	5.68	1.94

2.4 Governing Equations

In the CFD simulation, pathogen transmission is modelled as the particles that is emitted to the surrounding medium of air. Thus, it is crucial to establish the flow field to reproduce the physical condition of the transmission, as the discrete phase (Lagrangian model) interacts with the continuous phase (Eulerian model). In the Eulerian phase, the continuity equation is expressed in Eq. (4). The first term of the equation defines the transient flow field, while the remaining terms expresses the location of particles in x, y, and z direction.

$$\frac{\partial \rho}{\partial t} + \frac{\partial}{\partial x_i}(\rho u_i) + \frac{\partial}{\partial y_j}\left(\rho u_j\right) + \frac{\partial}{\partial z_k}(\rho u_k) = 0 \tag{4}$$

In addition, the Navier-Stokes equation can be presented in terms of the local acceleration $\rho \frac{\partial \vec{v}}{\partial t}$, convective acceleration $\rho(\vec{v} \cdot \nabla)\vec{v}$, pressure gradient $-\nabla P$, body force term $\vec{\gamma}\rho$, and viscous term $\mu\nabla^2\vec{v}$. Each term collectively forming into Eq. (5).

$$\rho \frac{\partial \vec{v}}{\partial t} + \rho(\vec{v} \cdot \nabla)\vec{v} = -\nabla P + \vec{\gamma}\rho + \mu\nabla^2\vec{v} \tag{5}$$

In turbulence flow field condition, the kinetic energy of the turbulence flow nature is expressed in Eq. (6). Turbulent kinetic energy, k defined in m^2/s^2, turbulent dissipation rate, ε in m^2/s^3, and G_k which is the turbulent kinetic energy bounded by the mean velocity gradient.

$$\frac{\partial}{\partial t}(\rho k) + \nabla \cdot (\rho k \vec{u}) = \nabla \cdot \left[\mu + \frac{u_t}{\sigma_k}\nabla k\right] + G_k - \rho\varepsilon \tag{6}$$

Behaviour of particles can be modelled by considering the forces acting on the particles. In this case, the Eq. (7) is used to express the particle motion. In the equation, the term $\overrightarrow{u_p}$ represents the particle velocity vector, $\vec{u}$ denotes the velocity of the continuous phase, $\vec{F}$ expresses the additional forces, while $\rho_p$and ρ represents the particle density and fluid density respectively. In the present study, the injected particles are modelled as sphere-shaped element. Therefore, the drag force acting on the particles is expressed in Eq. (8) to account for the particle interaction with the continuous phase. The equation denotes relative Reynolds number as $R_e$and its corresponding drag coefficient as C_D.

$$\frac{d\vec{u}_p}{dt} = F_D(\vec{u} - \vec{u}_p) + \frac{\vec{g}(\rho_p - \rho)}{\rho_p} + \vec{F} \tag{7}$$

$$F_{drag} = F_D(\vec{u} - \overrightarrow{u_p}) = \frac{18\mu}{\rho_p d_p^2}\frac{C_D R_e}{24}(\vec{u} - \overrightarrow{u_p}) \tag{8}$$

2.5 Piecewise Validation of Simulation Model

Under ideal conditions, results from CFD simulation should be compared with experimental data. For the present study, the computational simulation will not be accompanied by the experimental works. However, the accuracy of the simulation results can be calculated by performing a piecewise validation to gain confidence on the result. This validation test is initiated by performing CFD analysis to one of the components of interest in the domain. In this case, the value of axial velocity of coughing jet produced from the fine mesh is compared to the solution value for infinitely fine mesh $(h = 0)$ calculated from Richardson extrapolation. In the test case, axial velocity value for each mesh level is measured at a point 14cm from the transmitter's mouth, as illustrated in Figure 5. The solution value for each coarse, medium and fine mesh is obtained and compared between the extrapolated solution, with the corresponding representative cell length and extrapolated error percentage as tabulated in Table 3 and as plotted in Figure 4.

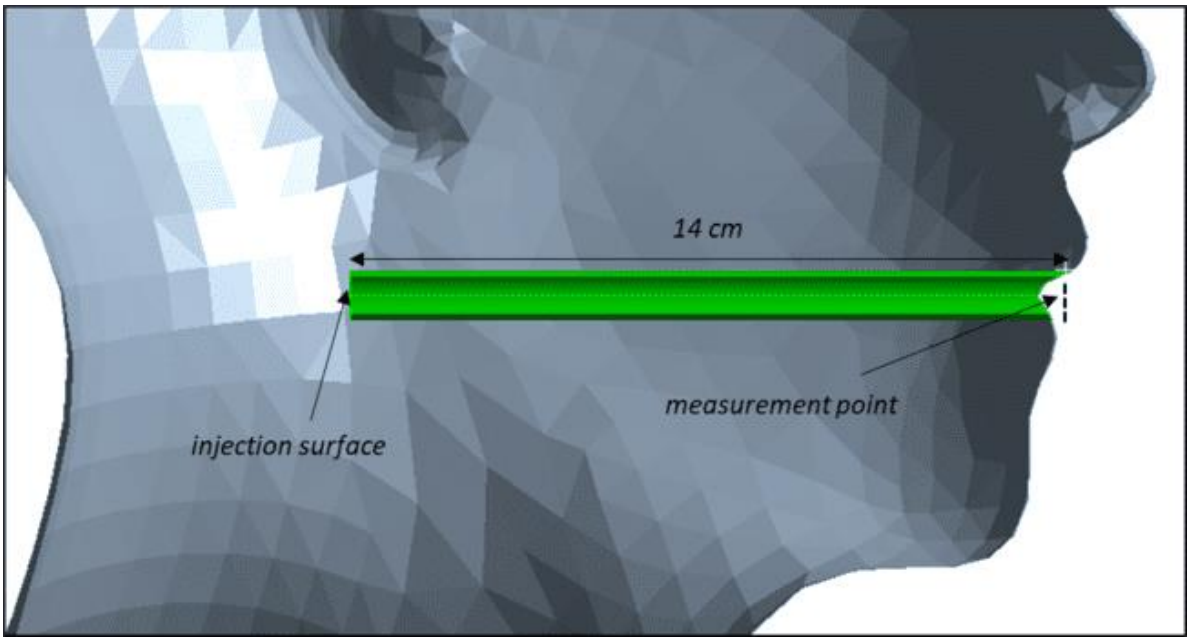

Fig. 5. Unit test at injector tube to calculate axial velocity

Table 3
Mesh sensitivity test result

Mesh Level	Representative cell length, h (mm)	Axial velocity (m/s)	Extrapolated relative error (%)
Fine	10.90	5.46	3.95
Medium	14.40	5.33	6.24
Coarse	19.12	5.12	9.93

3. Results

3.1 Velocity Contour Plot

It is crucial to observe the flow field of the entering wind inside the domain to better understand the transmission pattern in a closed space. Velocity contour plot is generated on vertical midplane of the domain at yz-plane to capture the flow field of each simulation case. Each case represents inlet wind velocity of 1.0 m/s (light air), 3.9 m/s (light breeze), and 5.5 m/s (moderate breeze) respectively at different time step of 0.5, 1.5, 2.5, and 4.5 s. From Figure 6 and Figure 7, the contour plot revealed the different flow field downstream of the transmitter and receiver mannequin in the domain. It is

observed that the flow field gets more intense as the incoming wind velocity increases. However, at wind velocity of 3.9 m/s, a noticeable difference can be observed for the wake behind the mannequin at t = 2.5 s and t = 4.5 s where the flow velocity is affected by the relative humidity of air. This is due to the higher moisture content in the air at higher humidity of 99.5%, as compared to lower humidity of 40%. At wind velocity of 5.5 m/s, the wake pattern observed to be stabilised, as the wind possesses sufficient force to propel forward, causing the effect of moisture content to be negligible.

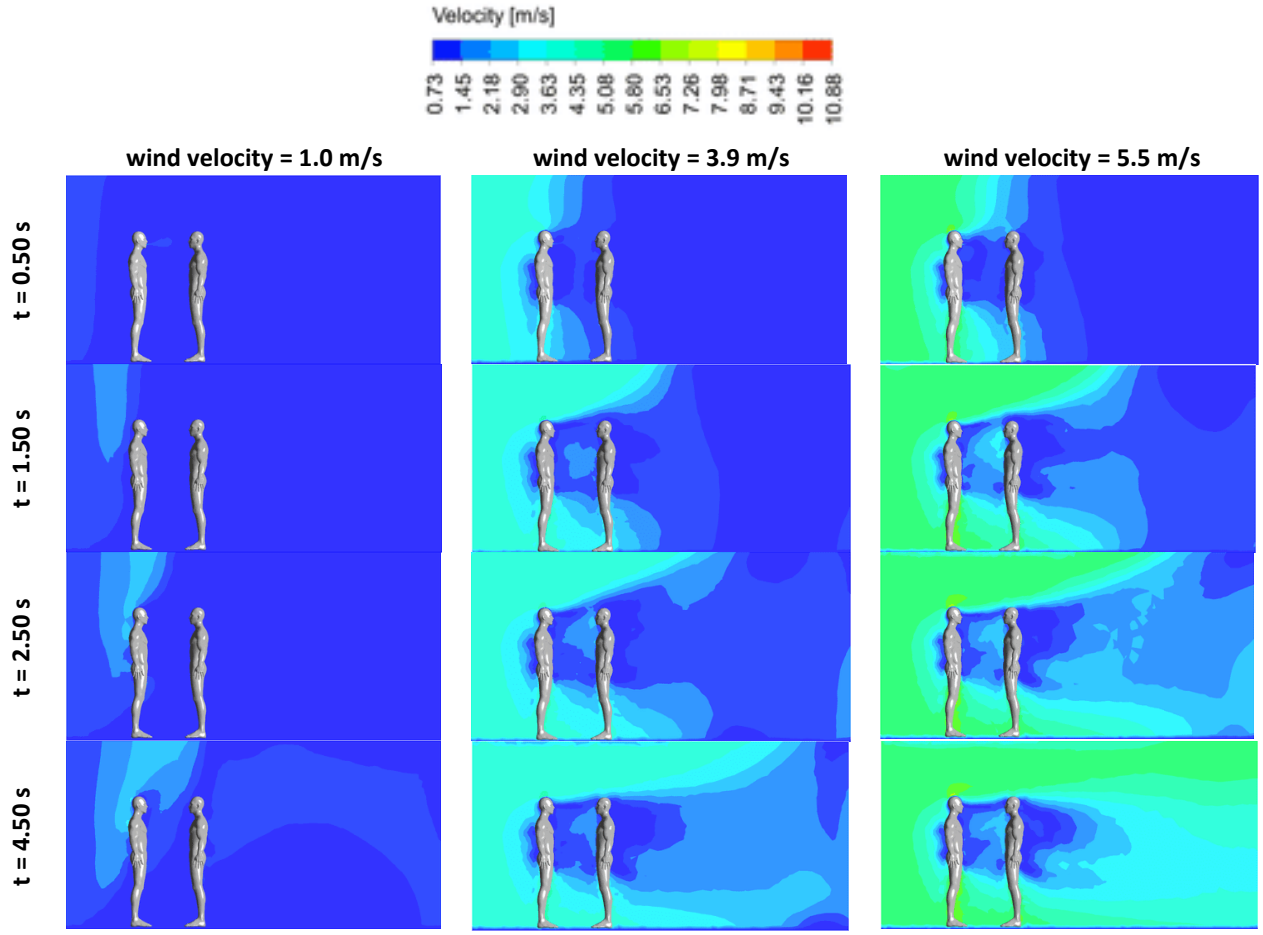

Fig. 6. Velocity contour generated from wind with relative humidity, RH = 40%, at 3 feet physical distance

Relative humidity parameter used in the present study is RH = 40% and RH = 99.5%. Lower relative humidity represents the average air humidity that is commonly used in the existing literatures. Both humidity level chosen to represent average humidity and extreme humidity level with high moisture content in the surrounding air. Further evidence of effect of humidity on airborne transmission is investigated to observe the sensitivity of airborne droplets emitting from coughing with respect to the humidity trend. Discrete phase model adopted in the study is defined as two-way turbulence coupling with interaction of Lagrange phase of the droplet with the continuous phase of air flow.

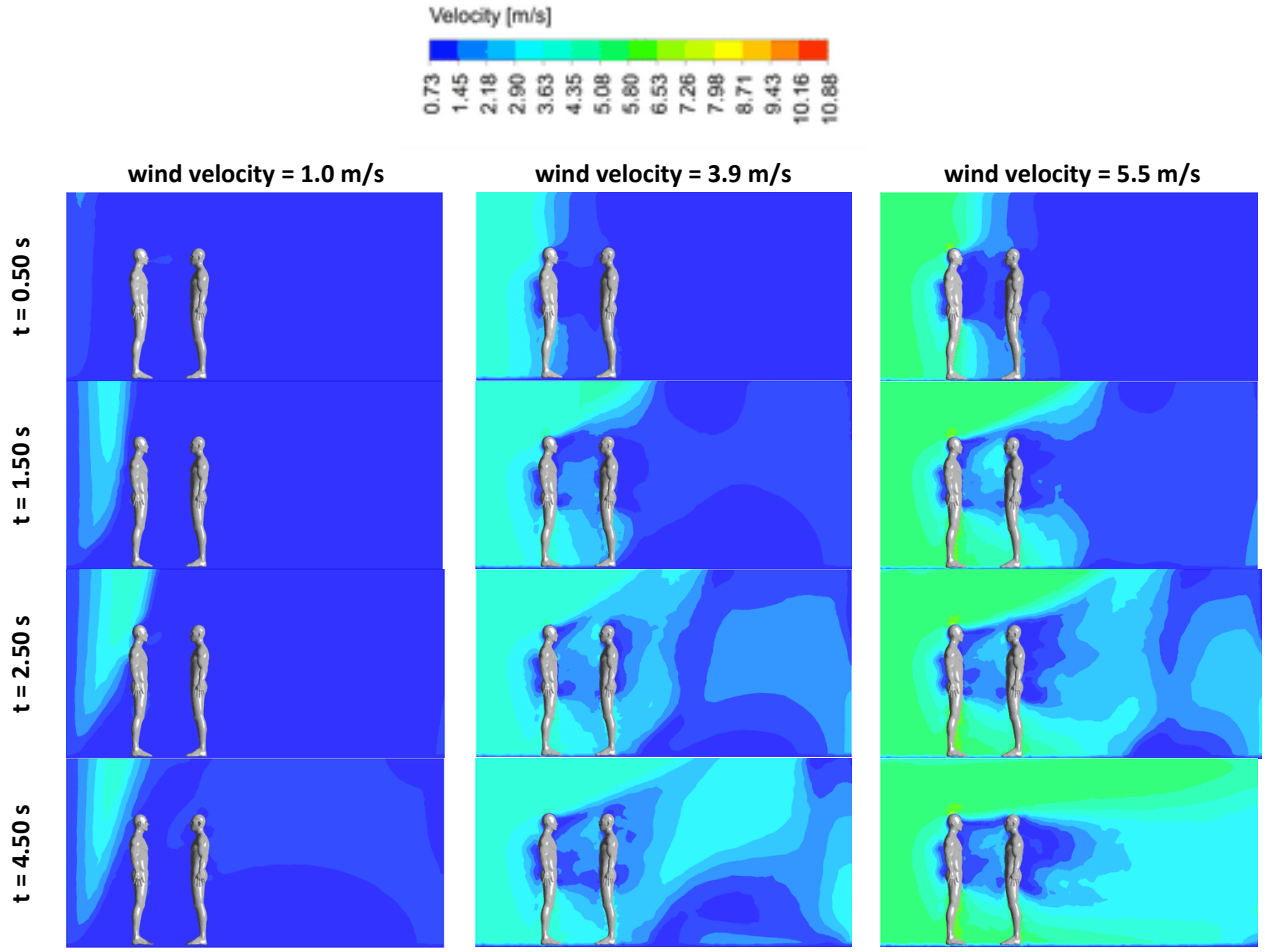

Fig. 7. Velocity contour generated from wind with relative humidity, RH = 99.5%, at 3 feet physical distance

3.2 Streamline Pattern

Streamline path of inlet wind is visualised as a supplementary to the velocity contour. It is observed that the streamline direction is analogous to the flow field as described from the flow contour and is able to reveal the region in the domain where the flow recirculation exists. The streamline patterns provide insights into the trajectories of the emitted airborne droplets. Figure 8 and Figure 9 illustrate the streamline path for each case of simulation.

From the streamline pattern generated, a region of flow recirculation is observed between the transmitter and receiver body. Streamline pattern showed increasing level of intensity with increasing velocity of incoming wind coming from behind the transmitter's body. Air flow is observed to be directed from in between the legs of transmitter up towards the torso region of the receiver.

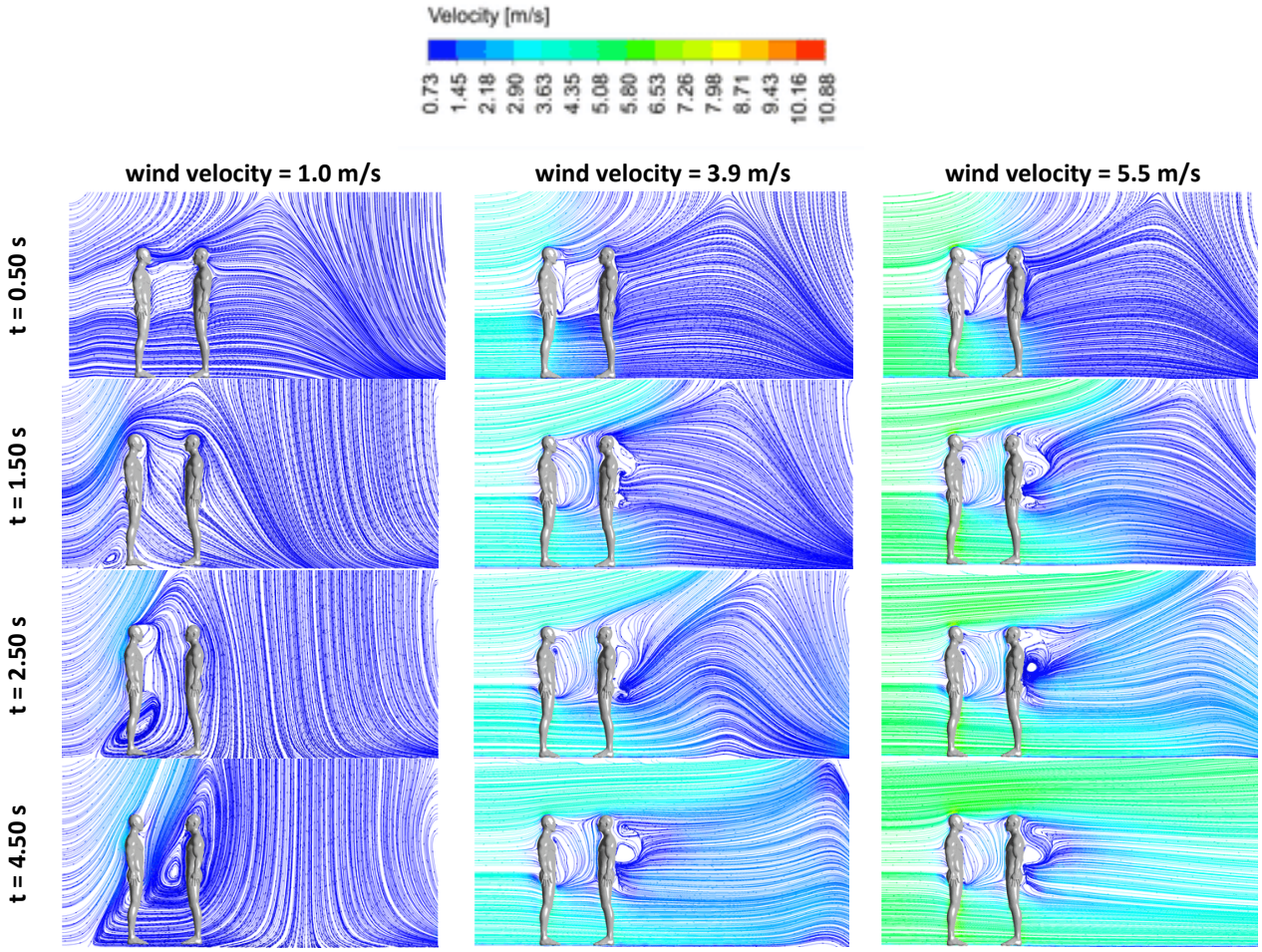

Fig. 8. Wind streamline direction at RH = 40%, at 3 feet physical distance

Simulation result showed that at 3 feet inter-personal distance between transmitter and receiver, flow recirculation puts the transmitter more at risk. This is due to recirculation of droplet particles to transmitter after the cough jet emission, instead of being propelled forward to the receiver. Furthermore, flow of droplets emitted will be restricted in the transverse direction (x-axis) of the computational domain. Increasing the distance between transmitter and receiver can potentially reduce the recirculation effect, as the recirculation flow path is further detached from the receiver body, thereby reducing exposure risk towards the receiver. This suggest that a shorter physical distance, both transmitter and receiver is equally exposed to the airborne transmission while at larger inter-personal distance, the transmitter receive higher exposure risk.

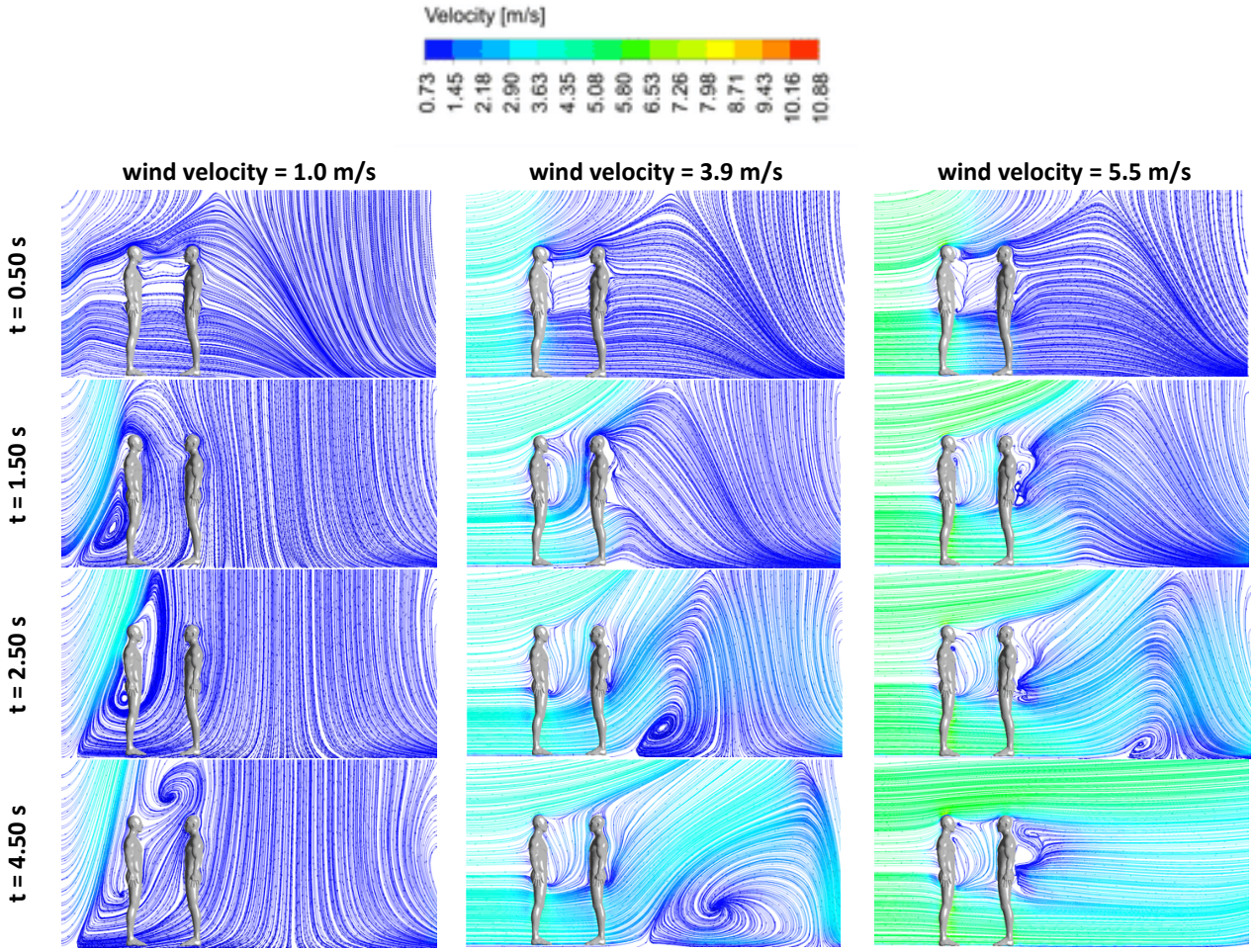

Fig. 9. Wind streamline direction at RH = 99.5%, at 3 feet physical distance

3.3 Droplets Transmission Pattern

Visualization of droplet particles emission is crucial to further understand its interaction with the surrounding flow field that is illustrated from both velocity contour plot and the streamline path. The droplet particles emitted from coughing is fitted with Rosin-Rammler curve, with two separate droplet distribution emitted at once. Size distribution of droplets consists of 1 to 50 µm range followed by 50 to 1000 µm range. Both particle size distribution is injected at t = 0.05 s up until t = 0.45s, to reproduce the coughing period range.

For droplet size distribution of 1 to 50 µm, the effect of relative humidity is more prominent for wind velocity of 3.9 m/s and 5.5 m/s. Droplets are observed to be more airborne and dispersed at lower humidity, compared to in higher humidity. This is due to the evaporation effect causing the droplet particles to shrink and eventually affecting its trajectory as time progress. In contrast, the droplets are heavier and less airborne due to the higher moisture content in the air. Furthermore, higher relative humidity of air leads to the clumping of the droplets causing it to travel at shorter distance as opposed to those particles in lower humidity. This phenomenon is due to the hygroscopic growth effect in a more humid air, which leads to increase in droplet size and its overall mass. Droplet particles transmission pattern in surrounding air of RH = 40% and RH = 99.5% is illustrated in Figure 10 and Figure 11 respectively.

Simulation result revealed that for particle size distribution of 50 to 1000 µm, the droplets is more likely to accumulate and settle to the ground lower for all cases of wind inlet velocity and air relative humidity. This is due to the fact that given its bigger size range which have affected its overall mass. Furthermore, droplets emitted from transmitter reaches the receiver within 0.5 s.

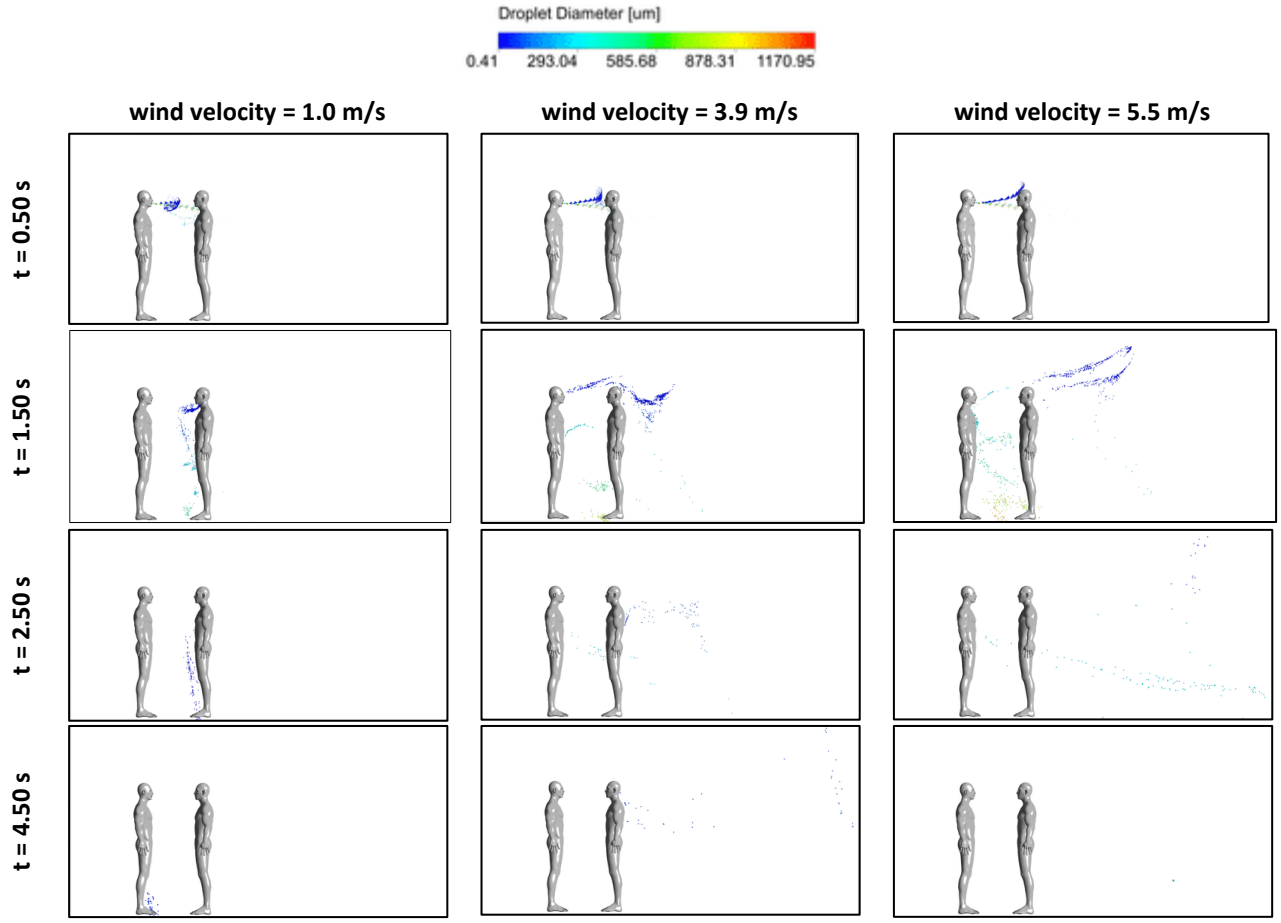

Fig. 10. Droplet diameter at different wind velocity in RH = 40%, at 3 feet physical distanc

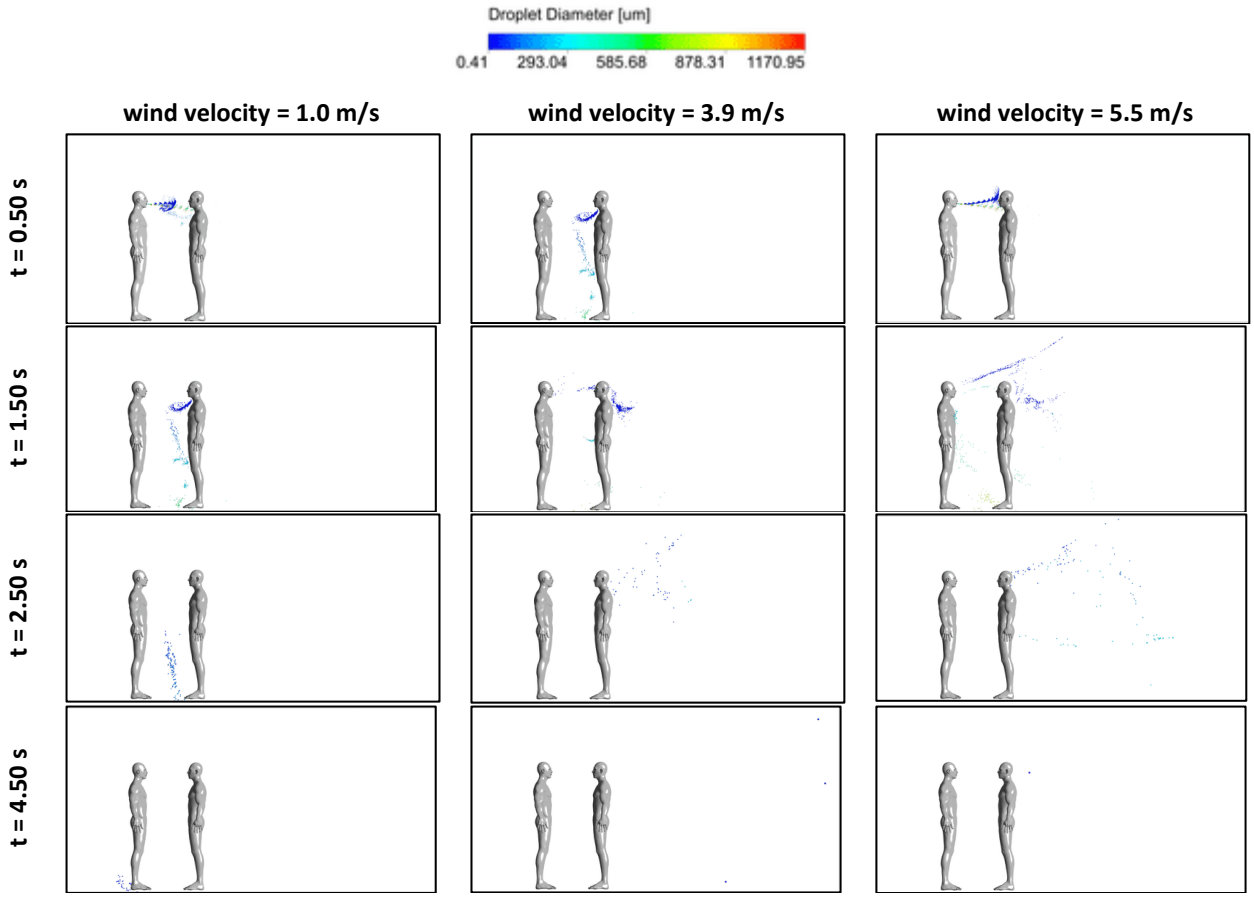

Fig. 11. Droplet diameter at different wind velocity in RH = 99.5%, at 3 feet physical distance

3.4 DPM Mass Source Analysis

Droplet particles injected from transmitter's mouth will be dispersed in the computational domain. The discrete phase model (DPM) mass source value for included boundary condition in the domain is calculated for each simulation case. Present study investigated droplets deposition at transmitter body, receiver body, and the floor. Hence, this section discussed on the DPM mass source plot at different inlet wind velocity and relative humidity.

3.4.1 Deposited mass at transmitter

From DPM concentration plot, highest deposited droplet mass observed at transmitter at t = 1.50 s. that there's a significant difference between the deposited mass at receiver in RH = 40% and RH = 99.5%, particularly at the highest wind speed. Hence, at high wind speed, the droplet transmission rate increases, contributed due to the accelerated convection effect in the space. This phenomenon is coupled with the low air humidity, allowing cough droplets to evaporate into smaller size particles making it easier for the recirculation region to redirect the droplets to the transmitter. Hence, the transmitter received the highest amount of droplets deposition at 3.9 m/s wind in a lower humidity. The DPM mass source plot is presented in Figure 12(a) to Figure 12(d).

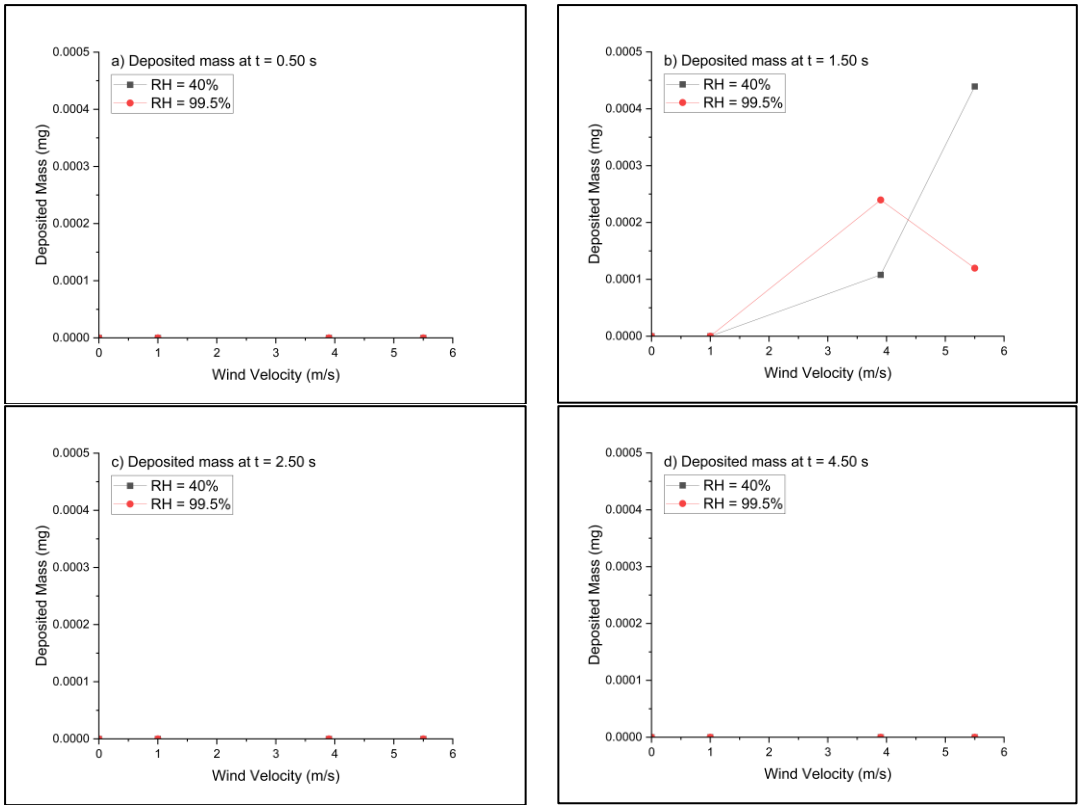

Fig. 12. Deposited droplet mass at transmitter body at 3 feet physical distance

3.4.2 Deposited mass at receiver

Similar quantitative variable is measured at receiver body. Since the receiver being in the downwind of the incoming wind direction and placed directly opposite to the transmitter, it is crucial to investigate the deposited mass of cough droplets that will potentially reach the receiver mannequin. It is observed that the receiver body received the highest mass deposition at 3.9 m/s wind speed in lower relative humidity of air. Similar to the case of transmitter deposition, the cough droplets pose higher infection risk towards the exposed person in moderate air speed as the evaporation effect contributed to the airborne nature of the evaporated droplets. At physical distance of 3 feet, the droplet deposition mass is significantly high within 0.5 s, suggesting that the inter-personal distance of 3 feet is insufficient in mitigating infection risk and the spread of virus-laden airborne pathogens. Figure 13(a)-(d) presents the droplet mass concentration at receiver body.

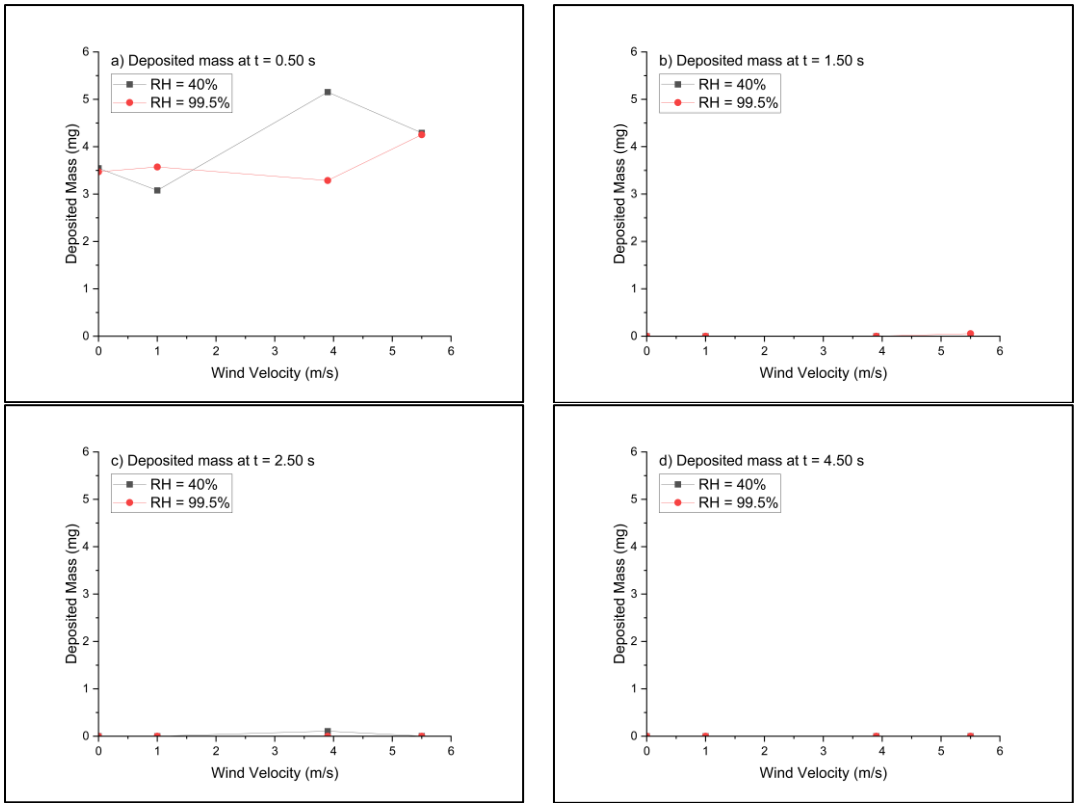

Fig. 13. Droplet mass concentration deposited at receiver body at 3 feet physical distance

3.4.3 Deposited mass on the floor

Gravitational force will influence how the cough droplets will fall to the ground at a certain transmission distance depending as a function of its size and mass. In a more humid air, the hygroscopic growth effect is greater compared to the evaporation effect. It is observed that there is significantly more cough droplet mass deposited onto the floor at t = 1.50 s. Due to the distance between transmitter and receiver, droplets will eventually fall onto the ground once they lose momentum and kinetic energy to travel further. For cases with 3 feet physical distance, droplets are directly deposited onto the nearby surface, and observed that the plotted results suggests that physical distance of 3 feet is ineffective in preventing deposition of virus particles onto the exposed subject. The comparison of droplet mass deposition at different time step for 3 feet physical distance is shown in Figure 14(a)-(d).

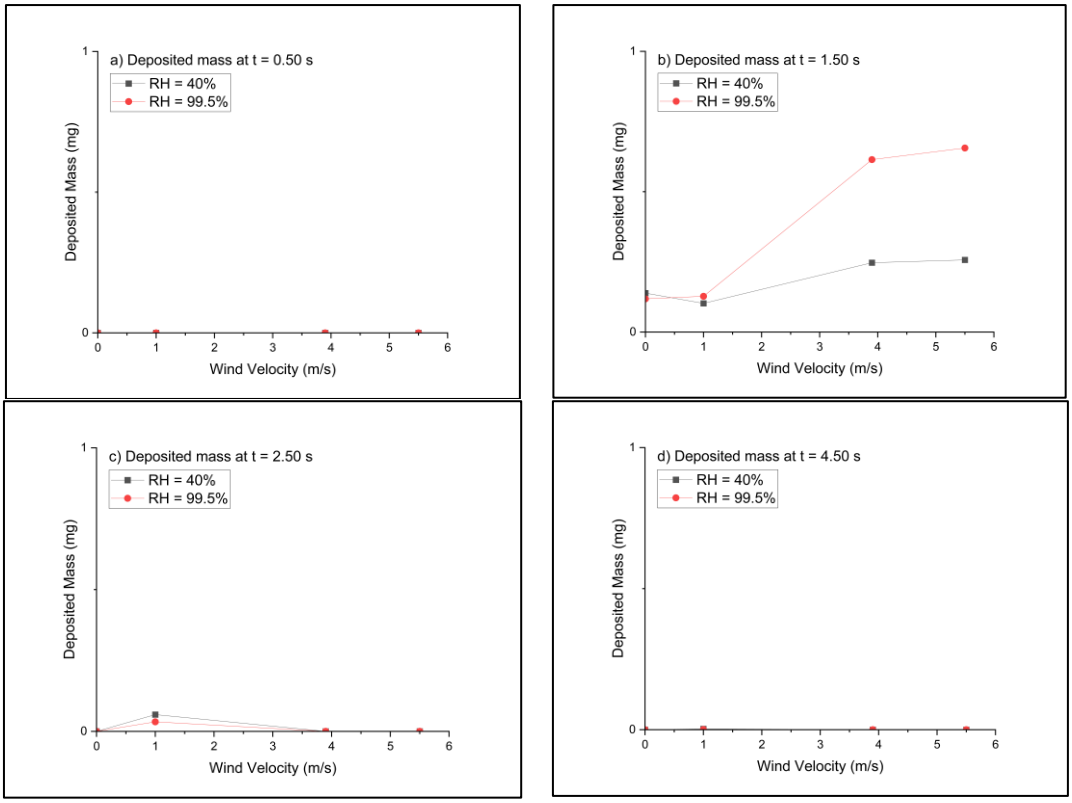

Fig. 14. Droplet mass concentration deposited on the floor at 3 feet physical distance

4. Conclusions

Airborne droplets transmission emitted from coughing in an enclosed space with horizontal inlet wind condition was simulated under transient simulation to study the behaviour of droplet deposition. Simulation result revealed that

i. Recirculation region generated from incoming wind in between transmitter and receiver causing droplet particles to be recirculated to the source, which is the transmitter.
ii. Droplets are observed to be more airborne and dispersed at lower humidity, compared to in higher humidity due to the evaporation effect causing the droplet particles to shrink.
iii. In a more humid air of higher moisture content, droplets are heavier and less airborne due to the hygroscopic growth effect which leads to increase in droplet size and its overall mass.
iv. In a 3 feet physical distance condition, receiver received highest mass deposition of 5.15 mg at t = 0.5 s under RH = 40% and in a light breeze wind condition of 3.9 m/s.
v. Higher number of droplet particles settle to the floor about 0.66 mg in higher relative humidity as compared to in lower humidity which only deposits around 0.26 mg of mass.
vi. Cough droplets deposited to the transmitter body at a higher mass of 0.00044 mg in lower humidity as compared to 0.00012 mg in higher humidity.

Acknowledgement
This research was sponsored by Ministry of Higher Education (MOHE) of Malaysia through Fundamental Research Grant Scheme (FRGS/1/2021/TK0/UTM/02/98).

References

[1] Milton, Donald K. "A Rosetta Stone for understanding infectious drops and aerosols." *Journal of the Pediatric Infectious Diseases Society* 9, no. 4 (2020): 413-415. https://doi.org/10.1093/jpids/piaa079

[2] Bhattacharyya, Suvanjan, Kunal Dey, Akshoy Ranjan Paul, and Ranjib Biswas. "A novel CFD analysis to minimize the spread of COVID-19 virus in hospital isolation room." *Chaos, Solitons & Fractals* 139 (2020): 110294. https://doi.org/10.1016/j.chaos.2020.110294

[3] Winata, I. Made Putra Arya, Putu Emilia Dewi, Putu Brahmanda Sudarsana, and Made Sucipta. "Air-Flow Simulation in Child Respirator for Covid-19 Personal Protection Equipment Using Bamboo-Based Activated Carbon Filter." *Journal of Advanced Research in Fluid Mechanics and Thermal Sciences* 91, no. 1 (2022): 83-91. https://doi.org/10.37934/arfmts.91.1.8391

[4] Ahad, Nor Aishah, Friday Zinzendoff Okwonu, and Pang Yik Siong. "COVID-19 Outbreak in Malaysia: Investigation on Fatality Cases." *Journal of Advanced Research in Applied Sciences and Engineering Technology* 20, no. 1 (2020): 1-10. https://doi.org/10.37934/araset.20.1.110

[5] Zhang, Zhihang, Taehoon Han, Kwang Hee Yoo, Jesse Capecelatro, André L. Boehman, and Kevin Maki. "Disease transmission through expiratory aerosols on an urban bus." *Physics of Fluids* 33, no. 1 (2021): 015116. https://doi.org/10.1063/5.0037452

[6] Xi, Jinxiang, Xiuhua April Si, and Ramaswamy Nagarajan. "Effects of mask-wearing on the inhalability and deposition of airborne SARS-CoV-2 aerosols in human upper airway." *Physics of Fluids* 32, no. 12 (2020): 123312. https://doi.org/10.1063/5.0034580

[7] Shah, Yash, John W. Kurelek, Sean D. Peterson, and Serhiy Yarusevych. "Experimental investigation of indoor aerosol dispersion and accumulation in the context of COVID-19: Effects of masks and ventilation." *Physics of Fluids* 33, no. 7 (2021): 073315. https://doi.org/10.1063/5.0057100

[8] Liu, Zhijian, Mo Zhang, Guoqing Cao, Song Tang, Haiyang Liu, and Liangqi Wang. "Influence of air supply velocity and room temperature conditions on bioaerosols distribution in a class I operating room." *Building and Environment* 204 (2021): 108116. https://doi.org/10.1016/j.buildenv.2021.108116

[9] Wong, Keng Yinn, Huiyi Tan, Bemgba Bevan Nyakuma, Haslinda Mohamed Kamar, Wah Yen Tey, Haslenda Hashim, Meng Choung Chiong et al. "Effects of medical staff's turning movement on dispersion of airborne particles under large air supply diffuser during operative surgeries." *Environmental Science and Pollution Research* 29, no. 54 (2022): 82492-82511. https://doi.org/10.1007/s11356-022-21579-y

[10] Hedworth, Hayden A., Mokbel Karam, Josh McConnell, James C. Sutherland, and Tony Saad. "Mitigation strategies for airborne disease transmission in orchestras using computational fluid dynamics." *Science Advances* 7, no. 26 (2021): eabg4511. https://doi.org/10.1126/sciadv.abg4511

[11] Ji, Yichen, Hua Qian, Jin Ye, and Xiaohong Zheng. "The impact of ambient humidity on the evaporation and dispersion of exhaled breathing droplets: A numerical investigation." *Journal of Aerosol Science* 115 (2018): 164-172. https://doi.org/10.1016/j.jaerosci.2017.10.009

[12] Komperda, Jonathan, Ahmad Peyvan, Dongru Li, Babak Kashir, Alexander L. Yarin, Constantine M. Megaridis, Parisa Mirbod et al. "Computer simulation of the SARS-CoV-2 contamination risk in a large dental clinic." *Physics of Fluids* 33, no. 3 (2021): 033328. https://doi.org/10.1063/5.0043934

[13] Mariam, Ashish Magar, Manish Joshi, Pachalla S. Rajagopal, Arshad Khan, Madhukar M. Rao, and Balvinder K. Sapra. "CFD simulation of the airborne transmission of COVID-19 vectors emitted during respiratory mechanisms: Revisiting the concept of safe distance." *ACS Omega* 6, no. 26 (2021): 16876-16889. https://doi.org/10.1021/acsomega.1c01489

[14] Cheong, Chang Heon, Beungyong Park, and Seong Ryong Ryu. "Effect of under-floor air distribution system to prevent the spread of airborne pathogens in classrooms." *Case Studies in Thermal Engineering* 28 (2021): 101641. https://doi.org/10.1016/j.csite.2021.101641

[15] MS 2680:2017. "Energy Efficiency and Use of Renewable Energy for Residential Buildings - Code of Practice." *Malaysian Standard* (2017).

[16] Chillón, Sergio A., Ainara Ugarte-Anero, Iñigo Aramendia, Unai Fernandez-Gamiz, and Ekaitz Zulueta. "Numerical modeling of the spread of cough saliva droplets in a calm confined space." *Mathematics* 9, no. 5 (2021): 574. https://doi.org/10.3390/math9050574

[17] World Health Organization. "COVID-19: Physical Distancing." *WHO*, 2021. https://www.who.int/westernpacific/emergencies/covid-19/information/physical-distancing.

[18] Zhang, Yixian, Guohui Feng, Yang Bi, Yilin Cai, Zheng Zhang, and Guangyu Cao. "Distribution of droplet aerosols generated by mouth coughing and nose breathing in an air-conditioned room." *Sustainable Cities and Society* 51 (2019): 101721. https://doi.org/10.1016/j.scs.2019.101721

[19] D'Alessandro, V., M. Falone, L. Giammichele, and R. Ricci. "Eulerian-Lagrangian modeling of cough droplets irradiated by ultraviolet-C light in relation to SARS-CoV-2 transmission." *Physics of Fluids* 33, no. 3 (2021): 031905. https://doi.org/10.1063/5.0039224

[20] Feng, Yu, Thierry Marchal, Ted Sperry, and Hang Yi. "Influence of wind and relative humidity on the social distancing effectiveness to prevent COVID-19 airborne transmission: A numerical study." *Journal of Aerosol Science* 147 (2020): 105585. https://doi.org/10.1016/j.jaerosci.2020.105585

[21] Liu, Jiaxing, Ming Hao, Shulei Chen, Yang Yang, Jian Li, Qi Mei, Xin Bian, and Kun Liu. "Numerical evaluation of face masks for prevention of COVID-19 airborne transmission." *Environmental Science and Pollution Research* 29 (2022): 44939-44953. https://doi.org/10.1007/s11356-022-18587-3

[22] Beer, T. "Beaufort wind scale." *Encyclopedia of Natural Hazards* (2013): 42-45. https://doi.org/10.1007/978-1-4020-4399-4_24

[23] Yang, Lin, Xiangdong Li, Yihuan Yan, and Jiyuan Tu. "Effects of cough-jet on airflow and contaminant transport in an airliner cabin section." *The Journal of Computational Multiphase Flows* 10, no. 2 (2018): 72-82. https://doi.org/10.1177/1757482X17746920

[24] Haghnegahdar, Ahmadreza, Jianan Zhao, and Yu Feng. "Lung aerosol dynamics of airborne influenza A virus-laden droplets and the resultant immune system responses: An in silico study." *Journal of Aerosol Science* 134 (2019): 34-55. https://doi.org/10.1016/j.jaerosci.2019.04.009

[25] Mat, Mohamad Nur Hidayat, Nor Zelawati Asmuin, Md Faisal Md Basir, Marjan Goodarzi, Muhammad Faqhrurrazi Abd Rahman, Riyadhthusollehan Khairulfuaad, Balasem Abdulameer Jabbar, and Mohd Shareduwan Mohd Kasihmuddin. "Influence of divergent length on the gas-particle flow in dual hose dry ice blasting nozzle geometry." *Powder Technology* 364 (2020): 152-158. https://doi.org/10.1016/j.powtec.2020.01.060

[26] Mat, Mohamad Nur Hidayat, Nor Zelawati Asmuin, Md Faisal Md Basir, Marjan Goodarzi, and Nor Halim Hasan. "Effect of impact force for dual-hose dry blasting nozzle geometry for various pressure and distance: an experimental work." *The European Physical Journal Plus* 135, no. 2 (2020): 260. https://doi.org/10.1140/epjp/s13360-020-00251-9

[27] Celik, Ishmail B., Urmila Ghia, Patrick J. Roache, and Christopher J. Freitas. "Procedure for estimation and reporting of uncertainty due to discretization in CFD applications." *Journal of fluids Engineering-Transactions of the ASME* 130, no. 7 (2008): 078001. https://doi.org/10.1115/1.2960953